CentennialScale Variability of the Atlantic Meridional Overturning Circulation in CMIP6 Models Shaped by Arctic–North Atlantic Interactions and Sea Ice Biases

Geophysical Research Letters

RESEARCH LETTER
10.1029/2024GL110791

Centennial-Scale Variability of the Atlantic Meridional Overturning Circulation in CMIP6 Models Shaped by Arctic–North Atlantic Interactions and Sea Ice Biases

Oliver Mehling[1], Katinka Bellomo[1,2], and Jost von Hardenberg[1,2]

[1]Department of Environment, Land and Infrastructure Engineering, Politecnico di Torino, Turin, Italy, [2]National Research Council of Italy, Institute of Atmospheric Sciences and Climate (CNR-ISAC), Turin, Italy

Key Points:

- We present a robust multi-model comparison of internal centennial-scale AMOC variability in state-of-the-art climate models
- A robust mechanism of Arctic–North Atlantic freshwater exchange is identified only in models that use the NEMO ocean component
- Sea ice cover biases in convective regions of the North Atlantic amplify AMOC variability and could provide an observational constraint

Supporting Information:

Supporting Information may be found in the online version of this article.

Correspondence to:

O. Mehling,
oliver.mehling@polito.it

Citation:

Mehling, O., Bellomo, K., & von Hardenberg, J. (2024). Centennial-scale variability of the Atlantic meridional overturning circulation in CMIP6 models shaped by Arctic–North Atlantic interactions and sea ice biases. *Geophysical Research Letters*, *51*, e2024GL110791. https://doi.org/10.1029/2024GL110791

Received 13 JUN 2024
Accepted 4 OCT 2024

Author Contributions:

Conceptualization: Oliver Mehling, Katinka Bellomo, Jost von Hardenberg
Formal analysis: Oliver Mehling
Funding acquisition: Katinka Bellomo, Jost von Hardenberg
Investigation: Oliver Mehling
Methodology: Oliver Mehling, Katinka Bellomo, Jost von Hardenberg
Software: Oliver Mehling
Supervision: Katinka Bellomo, Jost von Hardenberg
Visualization: Oliver Mehling
Writing – original draft: Oliver Mehling

Abstract Climate variability on centennial timescales has often been linked to internal variability of the Atlantic Meridional Overturning Circulation (AMOC). However, due to the scarceness of suitable paleoclimate proxies and long climate model simulations, large uncertainties remain on the magnitude and physical mechanisms driving centennial-scale AMOC variability. For these reasons, we perform a systematic multi-model comparison of centennial-scale AMOC variability in pre-industrial control simulations of state-of-the-art global climate models. Six out of nine models in this study exhibit a statistically significant mode of centennial-scale AMOC variability. Our results show that freshwater exchanges between the Arctic Ocean and the North Atlantic provide a plausible driving mechanism in a subset of models, and that AMOC variability can be amplified by ocean–sea ice feedbacks in the Labrador Sea. The amplifying mechanism is linked to sea ice cover biases, which could provide an observational constraint for centennial-scale AMOC variability.

Plain Language Summary Changes in ocean circulation are often proposed as drivers of natural variations of the Earth's climate on timescales of centuries. However, it is unclear how strong these natural variations of the circulation strength, called internal variability, are in the real world, because reconstructions from the past climate are sparse and climate models are expensive to run for these long timescales. Here, we compare how the latest generation of climate models simulate internal variability of the Atlantic Meridional Overturning Circulation (AMOC)—the ocean circulation that is often thought to be responsible for Europe's comparatively mild climate—on timescales of 100–250 years. We find that many models have stronger variability on these timescales than what would be expected simply from random noise. In several models, AMOC variability appears to be driven by the release of fresh water from the Arctic Ocean and amplified by intermittent sea ice cover in the North Atlantic. However, this amplification only occurs if a model simulates a too extensive sea ice cover in winter. This mechanism shows that sea ice cover—which is easily observable—could be used to constrain variability of the AMOC on timescales longer than the observational record.

1. Introduction

Past and future climate change is determined by both external forcing (such as increasing anthropogenic CO_2 emissions or volcanic eruptions) and internal variability that arises from chaotic interactions between the different components of the climate system. Hence, assessing the magnitude of and mechanisms responsible for internal variability is crucial for regional climate projections (e.g., Lehner et al., 2020), detection and attribution (Eyring et al., 2021), and the interpretation of the paleoclimatic record (von der Heydt et al., 2021). While variability on interannual to decadal timescales can often be studied by combining large ensembles of climate models and the instrumental record, for longer timescales the uncertainty is much larger (Laepple et al., 2023) due to limited climate reconstructions and the computational cost of long climate model integrations.

Here, we focus on modes of climate variability on centennial timescales (defined as a period of 100–250 years), which have often been linked to internal variability of the Atlantic Meridional Overturning Circulation (AMOC) (e.g., Bakker et al., 2022; Ellerhoff et al., 2022; Knight et al., 2005; von der Heydt et al., 2021). Centennial-scale AMOC variability has been studied less extensively than the neighboring multidecadal timescales (Buckley & Marshall, 2016), but might still imprint on the climate at human timescales (e.g., Bonnet et al., 2021; Kelson et al., 2022). Because the AMOC strength is challenging to reconstruct from available sea surface temperature proxies (Bakker et al., 2022; Little et al., 2020; Moffa-Sánchez et al., 2019), and circulation proxies often do not

Writing – review & editing: Oliver Mehling, Katinka Bellomo, Jost von Hardenberg

provide sufficient resolution (Lippold et al., 2019), here we focus on simulated centennial-scale AMOC variability in state-of-the-art climate models.

In single climate model studies, several different mechanisms for a centennial-scale mode of AMOC variability have been suggested. Proposed drivers include the propagation of salinity anomalies from the southern hemisphere (Delworth & Zeng, 2012; Martin et al., 2015), subtropical precipitation anomalies (Vellinga & Wu, 2004), freshwater transport from the Arctic Ocean (Jiang et al., 2021; Meccia et al., 2023; Mehling et al., 2023), and internal ocean mixing feedbacks in the North Atlantic (Li & Yang, 2022; Prange et al., 2023; Yang et al., 2024). This diversity demonstrates a need for systematic model intercomparison of centennial-scale AMOC variability and its mechanisms, which—in contrast to shorter timescales (Ba et al., 2014; Muir & Fedorov, 2015)—has so far only been achieved with one very small (three-model) ensemble (Menary et al., 2012).

Here, we provide a robust systematic intercomparison of centennial-scale AMOC variability in the latest generation of global climate models, making use of the unprecedented availability of long pre-industrial control (piControl) simulations in the Coupled Model Intercomparison Project Phase 6 (CMIP6; Eyring et al., 2016). We also compare the link between Atlantic overturning and freshwater exchanges with the Arctic Ocean, which has previously been proposed as a driving mechanism of centennial-scale AMOC variability in two of these CMIP6 models (Jiang et al., 2021; Meccia et al., 2023). Finally, we discuss inter-model spread with a focus on sea ice biases in the pre-industrial mean state, which may help constrain simulated centennial-scale variability.

2. Materials and Methods

2.1. CMIP6 Model Data

To analyze internal variability, we use piControl simulations from CMIP6, in which the external forcing is held constant at 1850 levels (Eyring et al., 2016), hence the time evolution is governed by internal dynamics. We select the longest piControl simulation for each model if it spans at least 1,000 years. This is to both sufficiently sample centennial-scale variability, and to separate internal variability from a residual model drift. For our analysis, we require that models provide at least the meridional overturning streamfunction (msftyz or msftmz), salinity (so), velocity (uo and vo), mixed layer depth (mlotst) and sea ice concentration (siconc) as output.

This yields a set of 9 models from 8 different modeling centers (Table S1 in Supporting Information S1), a small but diverse sample of the larger CMIP6 ensemble. All models analyzed here have a nominal ocean resolution of around 1° and therefore parametrize mesoscale ocean eddies. However, in contrast to CMIP5, all models resolve two ocean gateways west of Greenland, allowing for a more consistent (and more realistic) representation of Arctic–North Atlantic linkages (Zanowski et al., 2021). Following Jiang et al. (2021), we detrend all time series quadratically to account for (potentially non-linear) model drift.

2.2. Diagnostics

We define AMOC strength for each latitude as the maximum of the Atlantic meridional overturning streamfunction over depth (Buckley & Marshall, 2016) below 500 m. Note that, in some models, streamfunction output is computed on the native ocean model grid instead of along true parallels, but the grid distortion in these models is small at the latitudes analyzed here. Freshwater content in the Arctic Ocean is expressed in terms of the thickness of the water column above a reference salinity S_{ref} (Haine et al., 2015):

$$h_{fw}(x,y,t) = \int_{D(S_{ref})}^{0} \frac{S_{ref} - S(x,y,z,t)}{S_{ref}}\,\mathrm{d}z. \tag{1}$$

and freshwater transport into the Arctic through each strait is defined as

$$\Phi_{fw} = \iint \mathbf{u}\,\frac{S_{ref} - S}{S_{ref}} \cdot \mathrm{d}\mathbf{A}, \tag{2}$$

where $\mathbf{u}$ is the velocity across a section of area $\mathrm{d}\mathbf{A}$ (pointing into the Arctic Ocean) (Zanowski et al., 2021, and references therein). The integral is taken over the full ocean depth and horizontal extent of the strait. Sections are calculated on the native model grids, using the definitions of Zanowski et al. (2021) where applicable.

Here, we choose the reference salinity as the volume-averaged Arctic Ocean mean salinity, delimited by the straits shown in Figure S1 of Supporting Information S1, for each model (Table S1 in Supporting Information S1). This approach has been taken in previous modeling studies (e.g., Cornish et al., 2020; Mehling et al., 2023) to account for different salinity biases of individual models. We tested that our results hold for the frequently used value of $S_{ref} = 34.8$ and are therefore not sensitive to the exact choice of S_{ref}. Defining the fingerprint in Figure 2 through freshwater content instead of depth-averaged salinity anomalies (Jiang et al., 2021; Meccia et al., 2023) yields a similar picture in the Arctic Ocean but avoids choosing an arbitrary reference depth as well as spuriously large anomalies in regions with shallow bathymetry.

Power spectra and coherency are computed using the multi-taper method (Percival & Walden, 2020; Thomson, 1982). To detect peaks in spectral power, we compare the spectra to the null hypothesis of a red noise spectrum generated by a first-order autoregressive (AR(1)) process (Mann & Lees, 1996). This method relies on smoothing the power spectrum before fitting an analytical AR(1) spectrum. Following the recommendations of Mann and Lees (1996), we choose the smoothing bandwidth parameter as $\Delta f_{smooth} = 0.05\ \text{year}^{-1}$, which yields a good overall match between the fit and the smoothed spectra. Our results are not sensitive to reasonable variations of Δf_{smooth}. For lagged regressions, we test significance using the method of Ebisuzaki (1997), controlling for multiple comparisons by using effective degrees of freedom (Mudelsee, 2014) based on the autocorrelation of both time series.

3. Results

3.1. Centennial-Scale AMOC Variability

First, we use power spectral analysis to show that a significant mode of variability in AMOC strength can be identified in several long control simulations of CMIP6 models. Since most models exhibit the strongest centennial-scale AMOC variability in depth space at around 40°N (Figure S2 in Supporting Information S1), we use the AMOC strength at 40°N to characterize AMOC variability in the following. However, on centennial timescales, the AMOC at 40°N is highly coherent (coherency >0.92 for all models in this study except ACCESS-ESM1-5) with the commonly used AMOC index at 26.5°N (Figure S3 in Supporting Information S1), such that the results do not strongly depend on the exact choice of latitude for the AMOC index.

Figure 1 shows the multi-taper power spectra of AMOC strength at 40°N as a function of the period, with the timescales of interest (period 100–250 years) highlighted in gray. Compared to the null hypothesis of an AR(1) process, six of the nine analyzed models exhibit a significant mode of AMOC variability on centennial timescales at the 99% confidence level. This includes all five models (IPSL-CM6A-LR, EC-Earth3, HadGEM3-GC31-LL, UKESM1-0-LL, CanESM5) that use NEMO as their ocean component (Table S1 in Supporting Information S1).

However, the amplitude and period of the peak spectral power of AMOC variability vary widely among models, with EC-Earth3 and IPSL-CM6A-LR showing stronger variability than the other models of the ensemble. Few models with a significant mode of variability show a clearly defined spectral peak at one timescale, but rather significant power across most of the 100–250 years range. Nevertheless, oscillations—although perhaps not as regular as for EC-Earth3 and IPSL-CM6A-LR—can be seen in the low-pass filtered time series in Figure S4 of Supporting Information S1 for all models with significant centennial-scale variability. Among these models, the standard deviation of the 70-year low-pass filtered time series ranges from 0.5 Sv for UKESM1-0-LL to 1.4 Sv for EC-Earth3. In the three remaining models, the low-pass filtered standard deviation is ≤0.5 Sv.

To understand whether the prevalence of significant centennial-scale AMOC variability is unique to the CMIP6 ensemble, we repeat the power spectral analysis for models from the LongRunMIP archive (Rugenstein et al., 2019) (Figure S5 in Supporting Information S1). This collection contains millennial-length piControl simulations mainly from models of the previous coupled model generation (CMIP5). Only one out of six CMIP5 models, CESM1, exhibits significant AMOC variability on multi-centennial timescales, as previously described by Yang et al. (2024). CNRM-CM6-1, another CMIP6 model that uses NEMO, also exhibits a strong, significant mode of AMOC variability on centennial timescales (Waldman et al., 2021) with a low-pass filtered standard deviation of 1.9 Sv. In contrast, the only CMIP5 model in the collection that used NEMO, IPSL-CM5A, does not have significant centennial-scale AMOC variability.

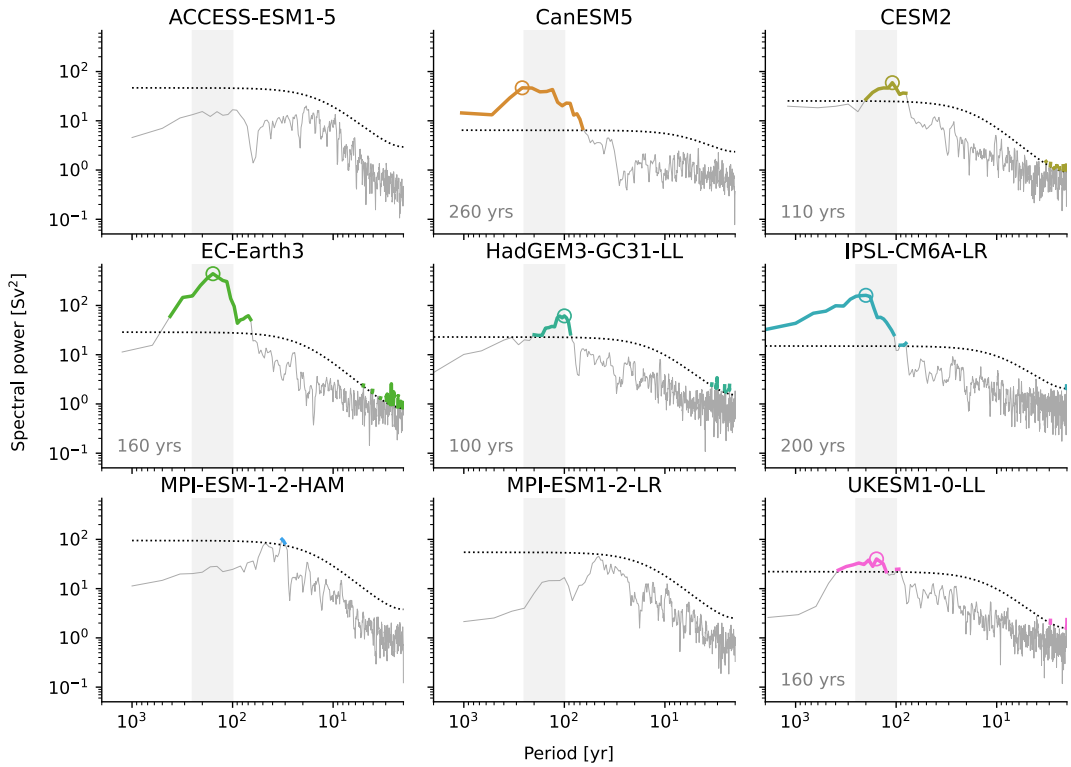

Figure 1. Power of centennial-scale AMOC variability. Multi-taper power spectra of detrended AMOC strength time series at 40°N for CMIP6 models with at least 1,000 years of piControl. Colored bands exceed the 99% confidence level (dotted line) of the AR(1) fit. For models with significant centennial-scale variability, unfilled circles and inset text show the period of maximum power (rounded to 10 years). Gray shading indicates the centennial timescale of interest in this paper (period 100–250 years).

3.2. Arctic–North Atlantic Freshwater Exchanges

To gain a mechanistic understanding of the drivers of this centennial-scale AMOC variability across climate models, we focus on one mechanism, Arctic–North Atlantic freshwater exchanges. This mechanism has been proposed to drive the AMOC oscillations in the IPSL-CM6A-LR and EC-Earth3 models (Jiang et al., 2021; Meccia et al., 2023). This focus is motivated not only by previous analysis of these two models, but also by coherence analysis of the AMOC strength by latitude (Figure S3 in Supporting Information S1). In all models, AMOC strength in the South Atlantic and equatorial Atlantic lags the AMOC at 40°N, and in all models except one (ACCESS-ESM1-5), the AMOC at 40–50°N leads that at 40°N. Hence, the northern high latitudes are a plausible driver of centennial-scale AMOC variability in almost all models.

Figure 2 shows one fingerprint of the Arctic–North Atlantic freshwater exchange mechanism—freshwater content changes in the Arctic Ocean instantaneously regressed onto the 70-year low-pass filtered AMOC. A very similar pattern was shown by Jiang et al. (2021) and Meccia et al. (2023) to induce a circulation anomaly that would trap freshwater in the central Arctic Ocean for some decades before releasing it to the North Atlantic and weakening the AMOC. We note that a similar Arctic salinity signature is also shown by Jungclaus et al. (2005) (their Figure 9), who proposed a very similar freshwater exchange mechanism except for shorter timescales.

Five of the nine models (IPSL-CM6A-LR, EC-Earth3, HadGEM3-GC31-LL, UKESM1-0-LL, CanESM5) have positive freshwater anomalies exceeding 1 m Sv^{-1} in the central Arctic Ocean and weaker negative freshwater anomalies elsewhere, in agreement with the pattern in Jiang et al. (2021) and Meccia et al. (2023). These five models match the subset of the ensemble that uses NEMO as its ocean component ("NEMO models" in the following for simplicity). Among NEMO models, there are differences in the response of the Beaufort Gyre, where HadGEM3-GC31-LL, UKESM1-0-LL and CanESM5 show a negative freshwater anomaly that opposes the central Arctic freshening, while the fresh anomalies in EC-Earth3 and IPSL-CM6A-LR extend toward the

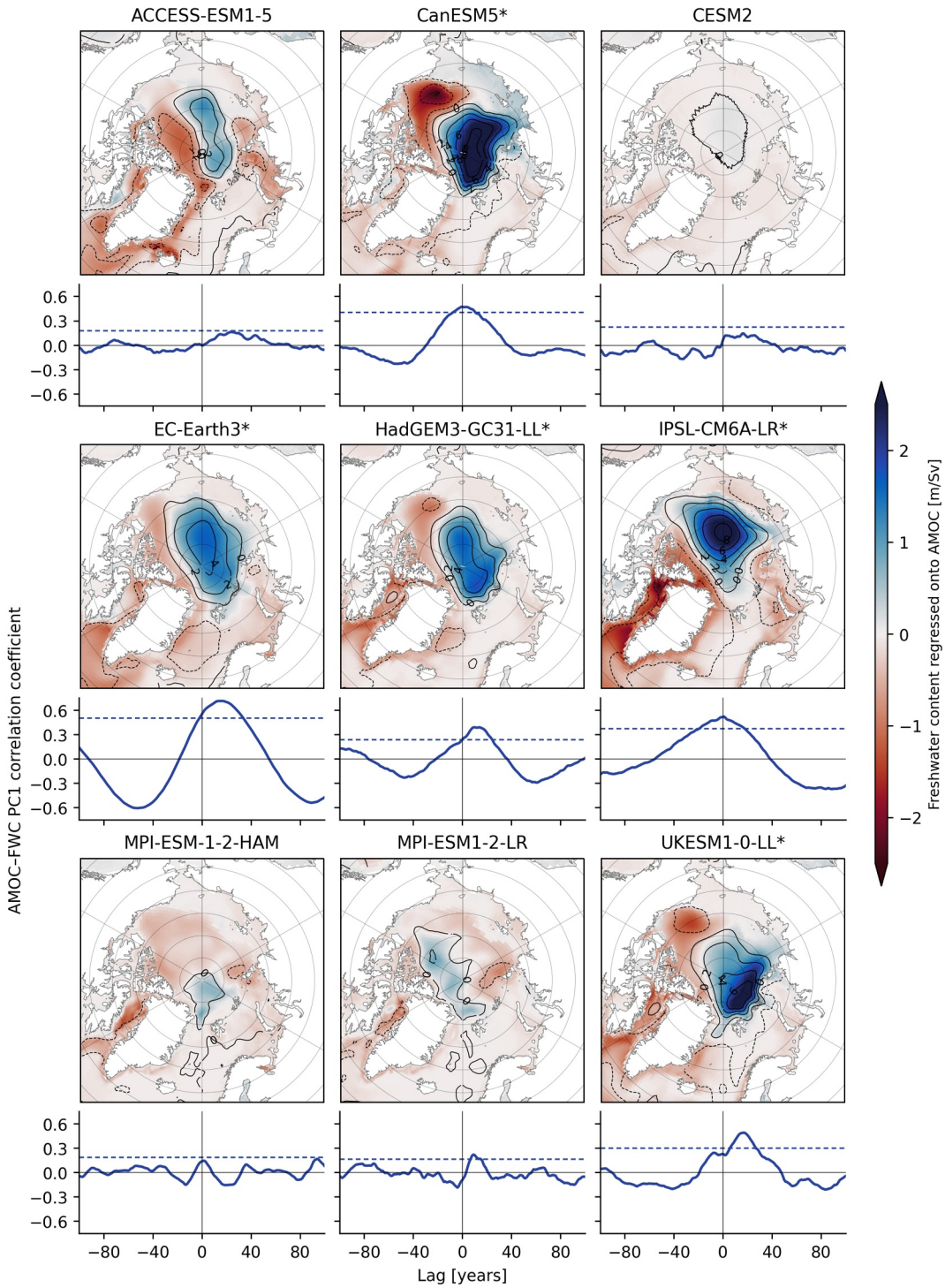

Figure 2. Fingerprint of the Arctic–North Atlantic freshwater mechanism. Maps: Low-pass filtered regression of freshwater content h_{fw} (colors, in m/Sv) and sea surface height (contours, in cm/Sv) onto AMOC strength for each model. Line plots: Lagged correlation between AMOC strength and the first principal component of annual mean Arctic Ocean freshwater content. Dashed lines indicate the (one-sided) 95% confidence level (see Section 2). While the maps are based on 70-year low-pass filtered time series, line plots are calculated from unfiltered annual means. NEMO models are indicated with an asterisk (*).

Beaufort Gyre. However, the central Arctic anomalies are the dominant contribution to the basin-integrated freshwater content anomaly in all five models (not shown). Among the four models that do not use NEMO, only ACCESS-ESM1-5 shows a similar freshwater regression pattern to the NEMO models when allowing for a

30-year lag behind the AMOC (Figure S6 in Supporting Information S1). All other models show only a weak (<1 m Sv^{-1} everywhere) and spatially inhomogeneous Arctic freshwater response to AMOC changes.

The model grouping is supported by empirical orthogonal function (EOF) analysis of the annual mean Arctic freshwater content fields. The first EOF (Figure S7 in Supporting Information S1), which explains between 20% and 50% of the variance depending on the model, is in good agreement with the regression patterns in Figure 2. The line plots in Figure 2 show the amplitude of this first EOF (i.e., the first principal component, PC1) correlated against the AMOC strength at 40°N. In all NEMO models, the maximum of the freshwater content PC1 is in phase or lags the AMOC by up to 20 years, while the lag for ACCESS-ESM1-5 is about 30 years. Strikingly, the correlation between AMOC and the Arctic freshwater content PC1 is significant at the 95% confidence level for all NEMO models, and the centennial timescale is clearly visible even without applying a low-pass filter. In contrast, in the non-NEMO models, the PC1–AMOC correlation is consistently weaker than in the NEMO models and mostly not significant, and the lagged correlation does not show a clear centennial timescale. Therefore, it is possible that the significant AMOC variability in CESM2 is generated by a mechanism linked to changes at lower latitudes, similar to mechanisms of multi-centennial variability found in its predecessor CESM1 (Li & Yang, 2022; Yang et al., 2024).

In all models, freshwater anomalies in the Arctic Ocean induce a corresponding change in sea surface height (contours in Figure 2), in line with the expectation that Arctic density anomalies, and therefore steric sea level anomalies, are dominated by salinity changes. While we cannot show velocity vectors for all models because angle information is not available in CMIP6 output, we expect that these sea surface height anomalies induce an anticyclonic geostrophic circulation anomaly as in Jiang et al. (2021). This anomaly provides a positive feedback that can prolong the period of the oscillations compared to theoretical expectations that Arctic–North Atlantic inter-basin exchanges should provide oscillations with a multi-decadal period (Wei & Zhang, 2022).

To verify that the freshwater anomalies are indeed a plausible driver of AMOC variability, we evaluate the freshwater transport across Fram Strait. In all NEMO models, the poleward freshwater transport consistently leads the AMOC strength by 20–30 years (Figure S8 in Supporting Information S1). Since the mean freshwater transport across Fram Strait is negative (i.e., southward) and dominated by the fresh near-surface East Greenland Current in all models, this implies that the liquid freshwater export from the Arctic Ocean is at its minimum 20–30 years before the AMOC maximum, consistent with the mechanism that an increased southward freshwater transport can weaken the AMOC with a lag, and vice versa (e.g., Dodd et al., 2009; Wei & Zhang, 2022; Zhang & Thomas, 2021). In three other models (ACCESS-ESM1-5, CESM2, MPI-ESM1-2-LR) the freshwater transport through Fram strait is also significantly correlated with the AMOC but with a shorter lag (5–10 years). The normalized magnitude (freshwater transport anomaly per Sverdrup of AMOC change) is stronger in the NEMO models and ACCESS-ESM1-5 than in the three remaining models.

3.3. Sea Ice Feedbacks Amplifying AMOC Variability

One intriguing similarity across NEMO-based models and ACCESS-ESM1-5 is the normalized (by the magnitude of AMOC variability) magnitude of the freshwater content (Figure 2) and transport (Figure S8 in Supporting Information S1), while the absolute magnitude of AMOC variability varies strongly between models (Figure 1). This suggests that feedbacks outside of the Arctic Ocean might amplify the centennial-scale AMOC variability in some models.

Here, we show that sea ice cover feedbacks in the Labrador Sea amplify AMOC variability at least in the two models with the strongest centennial-scale variability, EC-Earth3 and IPSL-CM6A-LR. In these models, sea ice in March covers the entire Labrador Sea during a weak AMOC phase, inducing a temporary collapse of Labrador Sea convection (Döscher et al., 2022, and Figures 3a and 3c). In contrast, during a strong AMOC phase, the sea ice edge retreats to within the Labrador Sea and the mixed layer reaches more than 700 m south of the ice edge. This provides a positive feedback for AMOC strength: weakening of the AMOC cools the North Atlantic, which leads to an extension of sea ice further into the Labrador Sea, which shuts down convective activity near the former ice edge, weakening the AMOC further. Similar feedbacks have been described in the literature for AMOC variability in colder climates (e.g., Klockmann et al., 2018).

Models like HadGEM3-GC31-LL and UKESM1-0-LL, which are characterized by weaker centennial-scale AMOC variability, also show a strong shallowing of the Labrador Sea winter mixed layer during the weak

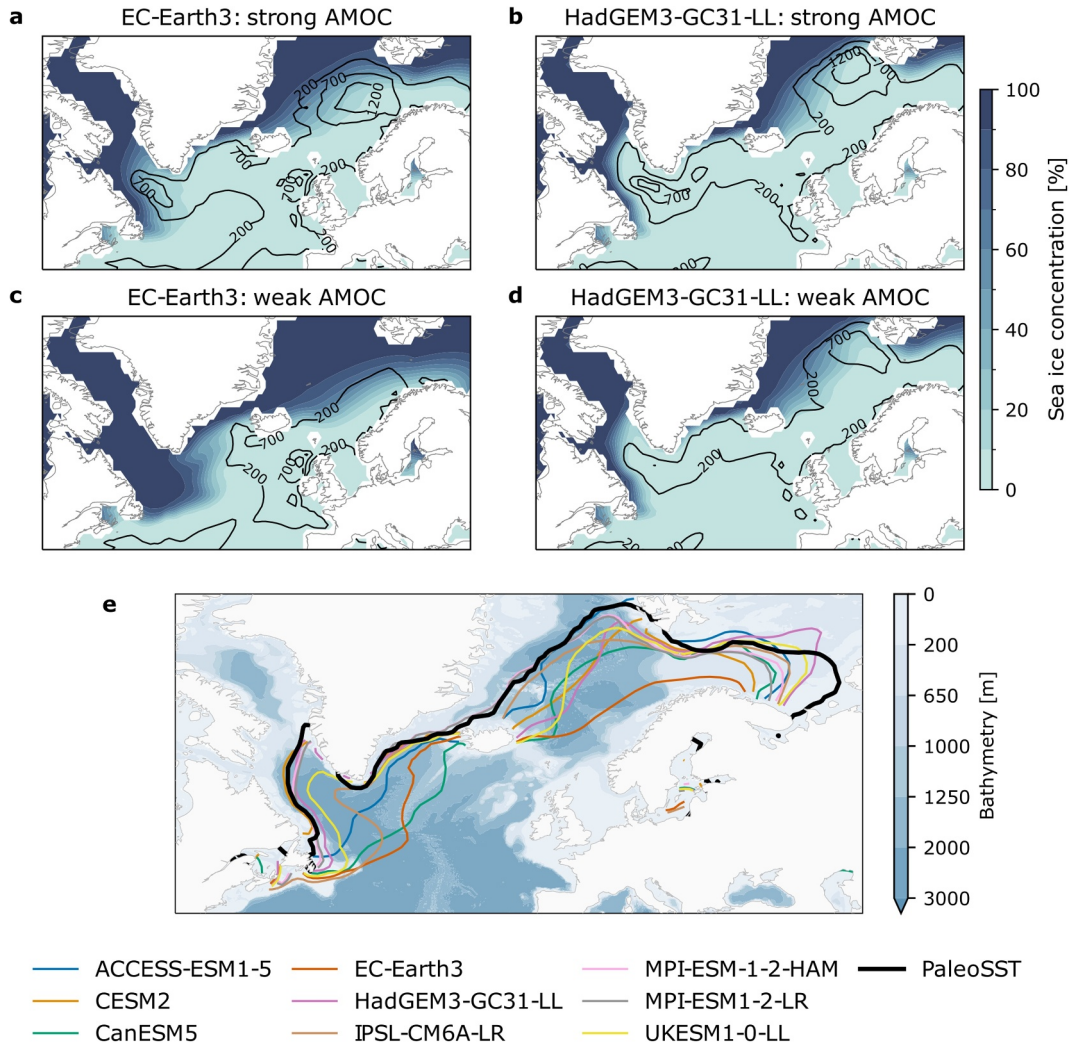

Figure 3. Role of the winter sea ice edge for centennial-scale AMOC variability. (a–d) Composites of mixed layer depth (contours) and sea ice concentration (color shading) in March for two models: (a, c) EC-Earth3 and (b,d) HadGEM3-GC31-LL. Composites are averaged over the strong and weak AMOC phases, which correspond to the intervals in which the low-pass filtered AMOC time series exceeds (Figure S4 in Supporting Information S1) plus or minus one standard deviation. Composites for all other models are shown in Figure S9 of Supporting Information S1. (e) Mean sea ice edge in March (contours; defined as the contours of 15% sea ice concentration) for CMIP6 models compared to the PaleoSST reconstruction (Samakinwa et al., 2021, black). The bathymetry (GEBCO Bathymetric Compilation Group, 2023) is shown in the background. Note that the sea ice edge biases in panel (e) are very similar when evaluated compared to observations over the historical period (1850–2014, Figure S11 in Supporting Information S1).

AMOC phase as expected. However, they exhibit little sensitivity of the sea ice edge to the change in AMOC strength (Figures 3b and 3d and Figure S9 in Supporting Information S1). This view is confirmed by the lagged regression of sea ice area and mixed layer depth in a box containing the Labrador Sea (48–64°N, 63–35°W) onto AMOC strength (Figure S10 in Supporting Information S1). Maximum mixed layer depth generally precedes the AMOC by some years and the sea ice minimum is approximately in phase with the AMOC. However, while the mixed layer deepening per Sv of AMOC change is similar between all models except for two outliers without Labrador Sea convection (see below), the sea ice sensitivity (area change per Sv of AMOC change) is much larger in EC-Earth and IPSL-CM6A-LR, and to some degree also in UKESM1-0-LL, than in all other models.

This difference in feedback strength between models can be linked to biases in the climatological mean position of the winter sea ice edge, defined as the contour of 15% sea ice concentration in March, in the Labrador Sea (Figure 3e). In HadGEM3, CESM2 and the MPI models, the pre-industrial mean sea ice edge in the Labrador Sea

is in proximity to the shelf break. This aligns well with gridded paleoclimate reconstructions for the period 1000–1849 (PaleoSST, Samakinwa et al., 2021). The proximity to the shelf break means that a retreat further north would not allow for more deep convection due to the shallow bathymetry, while the largest climatological mixed layer depths are located relatively far from the ice edge. In contrast, the mean ice edge position in UKESM1-0-LL, IPSL-CM6A-LR and EC-Earth3 is increasingly biased, reaching far into the Labrador Sea and even into the central North Atlantic in EC-Earth3. This bias allows for the AMOC–mixed layer–sea ice feedback described above, since a sea ice retreat opens areas in which deep convection can form. Two other models (ACCESS-ESM1-5 and CanESM5) also show a strong positive sea ice bias in the Labrador Sea, but do not form deep convection at any time in this region (cf. Heuzé, 2021). Instead, their deepest mixed layers in the North Atlantic are east of the Reykjanes Ridge (Figure S9 in Supporting Information S1). To summarize, the sea ice bias appears to be a necessary, but not sufficient, condition for strong centennial-scale AMOC variability.

In the Nordic Seas, only EC-Earth3 has a very pronounced positive sea ice bias compared to both reconstructions —far exceeding that of any other model of the ensemble –, which might explain its largest magnitude of AMOC variability (Figure 1). In EC-Earth3, deep convection can shut down simultaneously in the Labrador Sea and the Nordic Seas. Without the presence of deep-water formation in regions sufficiently far from the ice edge (e.g., in the Rockall Trough in EC-Earth3), the sea ice–mixed layer feedback could even lead to a near-shutdown of the AMOC, which has indeed been observed in earlier development versions of EC-Earth3 (Döscher et al., 2022) and also IPSL-CM6A-LR (Mignot et al., 2021).

It is therefore instructive to ask whether there is a link between strong centennial-scale AMOC variability and AMOC stability, as for example, suggested by the box model of Mehling et al. (2023). While it is not possible to test stability of CMIP6 models, we can compare their freshwater import into the South Atlantic (F_{ovS}), which has been proposed as an indicator for a mono- or bistable AMOC (de Vries & Weber, 2005; Drijfhout et al., 2011; Weijer et al., 2019) and is negative in observations (Arumí-Planas et al., 2024). According to the recent analysis of van Westen and Dijkstra (2024), CanESM5, EC-Earth3 and IPSL-CM6A-LR have an $F_{ovS} < 0$ typically associated with a bistable AMOC, whereas ACCESS-ESM1-5, CESM2, HadGEM3-GC31-LL, UKESM1-0-LL have an $F_{ovS} > 0$ associated with a monostable AMOC. However, the models with a negative F_{ovS} also have a positive sea ice bias, which might influence the F_{ovS}–bistability relation (van Westen & Dijkstra, 2023).

4. Discussion and Conclusions

In this study, we have provided a systematic multi-model comparison of centennial-scale AMOC variability, using long control simulations from CMIP6 models. Using a multi-model ensemble enabled probing the robustness of physical mechanisms, overcoming a main shortcoming of previous single-model studies. Six out of the nine models analyzed exhibit a significant mode of variability at centennial timescales, in line with previous studies which described strong centennial-scale AMOC variability for several individual CMIP6 models (Jiang et al., 2021; Meccia et al., 2023; Waldman et al., 2021). In contrast, only one out of six previous-generation CMIP5 models from the LongRunMIP archive (Rugenstein et al., 2019) had significant centennial-scale variability. We showed that a two-way interaction between AMOC strength and Arctic Ocean freshwater content provides a plausible mechanism for centennial-scale AMOC variability at least in the subset of CMIP6 models that use NEMO as their ocean component. This is consistent with the recent water mass analysis of Zhao et al. (2024) for multi-decadal AMOC variability in some of the same NEMO models, who found this variability to be mainly driven by the highest density classes associated with processes in the Arctic Ocean and GIN seas.

Interestingly, it has recently been shown that CMIP6 models that use NEMO simulate stronger Arctic Ocean warming and faster sea ice loss in future projections (Pan et al., 2023), pointing to a potential link between long-term variability and future Arctic change. Currently, it remains unclear which aspects of ocean model formulation (e.g., vertical mixing scheme), sea ice modeling (e.g., levitating vs. embedded sea ice) or tuning influence stronger variability (and sensitivity) in NEMO-based models in CMIP6. Clearly, there is a need for structured inter-model comparison of parametrization settings and for sensitivity experiments with perturbed parameters to answer the question of how model construction leads to differences in long-term AMOC behavior. Nevertheless, Shu et al. (2023) noted stronger volume transport and ocean heat transport into the Arctic Ocean through the BSO in NEMO-based ocean-only simulations, which could contribute to the stronger North Atlantic–Arctic links in Figure 2.

While several models in our study show a common mechanism, the magnitude of simulated centennial-scale AMOC variability differs strongly between models, even between those using a similar ocean model configuration. Our results suggest that this diversity is at least partly driven by differences in the sea ice mean state in the Labrador Sea, while other (not necessarily independent) mean state biases such as in high-latitude surface density have been shown to contribute as well (Zhao et al., 2024). In our ensemble, we showed for the first time that only models with a positive winter sea ice bias in the Labrador Sea can produce strong centennial-scale AMOC oscillations, provided that freshwater anomalies are transported in from the Arctic and that the model can temporarily form a deep mixed layer in the Labrador Sea when this sea ice retreats. In line with previous studies (Kim et al., 2023; Menary et al., 2015; Reintges et al., 2024), this highlights the need for an accurate simulation of the mean state in the subpolar North Atlantic as a prerequisite to reliably quantify AMOC variability. Biases in freshwater import into the South Atlantic (F_{ovS}) may also contribute to the presence or absence of oscillations, but further analysis of associated mechanisms is needed.

Since the amplitude of unforced centennial-scale AMOC variability is not an observable, selecting models with a realistic sea ice cover could be used to provide an observational constraint. Although such constraints should be corroborated with other lines of evidence, our analysis suggests that the simulated AMOC variability in IPSL-CM6A-LR and EC-Earth3 may be overestimated, which is in line with the results of Parsons et al. (2020) for global mean surface temperature variability. Alternatively, a more direct comparison of simulated variability with paleoclimate proxies would be possible using simulations of the last millennium (Jungclaus et al., 2017), as volcanic forcing can interfere with the unforced low-frequency variability (Cleveland Stout et al., 2023). Unfortunately, very few CMIP6 models have provided last millennium simulations so far.

If the magnitude of centennial-scale AMOC variability indeed depends on the position of the sea ice edge, we expect a weakening of centennial-scale variability as the sea ice edge retreats northward under global warming, although it might still be significant and even new amplifying mechanisms might become active (Mehling et al., 2023). For EC-Earth3, Meccia et al. (2023) indeed showed that the amplitude of centennial-scale AMOC variability is strongly reduced already under stabilization at moderately elevated CO_2 concentrations (Fabiano et al., 2024), in line with the mechanism proposed here. Whether this is also the case in other models has, to our knowledge, not yet been tested, but long AMOC time series from the LongRunMIP ensemble (Bonan et al., 2022) could be used in the future to compare centennial-scale AMOC variability under stronger greenhouse-gas forcing. Our analysis provides a physical mechanism for state-dependence (cf. Bellomo & Mehling, 2024) and we note that North Atlantic sea ice cover has also been invoked to explain the dependence of millennial-scale variability in the paleoclimate record on background CO_2 concentrations (Malmierca-Vallet et al., 2024, and references therein). On shorter (decadal) timescales, reduced AMOC variability under strong CO_2 forcing has been identified in a climate model (MacMartin et al., 2016), but it was linked to the weaker AMOC mean-state rather than sea ice changes. Regardless of the mechanism, state-dependence of AMOC variability would render detection and attribution of AMOC changes more difficult if internal variability is derived from pre-industrial control simulations (e.g., Kelson et al., 2022) and is therefore an important topic for future research.

While we used a small but relatively diverse sample of CMIP6 models, one caveat is that all models in this study (and most models in CMIP6) use a relatively coarse ocean resolution of about 1°. Recently, Patrizio et al. (2023) showed that 1° models are more salinity-stratified in the North Atlantic than their higher-resolution (1/4°) counterparts. Hence, freshwater anomalies propagating from the Arctic would be expected to influence density anomalies less strongly in higher-resolution models, and the centennial-scale AMOC variability might be weaker in these more realistic setups. However, a systematic comparison of low- and high-resolution models will be necessary to test this hypothesis. Finally, while the transport pathways shown in this study are physically plausible (lagged) correlations do not demonstrate causation. To this end, future studies could use more physics-based analyses, for example, through Lagrangian tracers or targeted sensitivity experiments.

To conclude, our results indicate that significant centennial-scale AMOC variability is relatively common among CMIP6 models, but that—just like on multidecadal timescales (Buckley & Marshall, 2016; Muir & Fedorov, 2015)—its magnitude varies widely across models. However, process understanding can guide to observables that could aid constraining simulated variability. To this end, our work identified two quantities of interest: the correlation between AMOC strength and Arctic Ocean freshwater content (Section 3.2) as well as the mean state of sea ice cover in the North Atlantic (Section 3.3). While the former might still be difficult to observe,

sea ice mean-state biases in the North Atlantic could contribute to observationally constrain simulated AMOC variability on timescales beyond the still relatively short observational record.

Data Availability Statement

All CMIP6 data used in this analysis is freely available from the Earth System Grid Federation (https://esgf-data.dkrz.de/projects/cmip6-dkrz/). Individual data sets are listed in the Table S1 of Supporting Information S1. The PaleoSST reconstruction was obtained from https://doi.org/10.6084/m9.figshare.c.5369309 (Brönnimann et al., 2021). Code and notebooks to reproduce the diagnostics are available at https://github.com/omehling/centennial-variability-CMIP6 and archived at https://doi.org/10.5281/zenodo.11640570 (Mehling, 2024).

Acknowledgments
OM and JvH have received funding from the European Union's Horizon 2020 research and innovation programme under the Marie Skłodowska-Curie grant agreement No. 956170 (CriticalEarth). KB has received funding from the European Union's Horizon 2020 research and innovation programme under the Marie Skłodowska-Curie grant agreement No. 101026907 (CliMOC). We acknowledge the World Climate Research Programme, which, through its Working Group on Coupled Modelling, coordinated and promoted CMIP6. We thank the climate modeling groups for producing and making available their model output, the Earth System Grid Federation (ESGF) for archiving the data and providing access, and the multiple funding agencies who support CMIP6 and ESGF. We also wish to thank the three reviewers whose comments have significantly improved the paper.

References

Arumí-Planas, C., Dong, S., Perez, R., Harrison, M. J., Farneti, R., & Hernández-Guerra, A. (2024). A multi-data set analysis of the freshwater transport by the Atlantic meridional overturning circulation at nominally 34.5°S. *Journal of Geophysical Research: Oceans*, *129*(6), e2023JC020558. https://doi.org/10.1029/2023JC020558

Ba, J., Keenlyside, N. S., Latif, M., Park, W., Ding, H., Lohmann, K., et al. (2014). A multi-model comparison of Atlantic multidecadal variability. *Climate Dynamics*, *43*(9–10), 2333–2348. https://doi.org/10.1007/s00382-014-2056-1

Bakker, P., Goosse, H., & Roche, D. M. (2022). Internal climate variability and spatial temperature correlations during the past 2000 years. *Climate of the Past*, *18*(11), 2523–2544. https://doi.org/10.5194/cp-18-2523-2022

Bellomo, K., & Mehling, O. (2024). Impacts and state-dependence of AMOC weakening in a warming climate. *Geophysical Research Letters*, *51*(10), e2023GL107624. https://doi.org/10.1029/2023GL107624

Bonan, D. B., Thompson, A. F., Newsom, E. R., Sun, S., & Rugenstein, M. (2022). Transient and equilibrium responses of the Atlantic overturning circulation to warming in coupled climate models: The role of temperature and salinity. *Journal of Climate*, *35*(15), 5173–5193. https://doi.org/10.1175/JCLI-D-21-0912.1

Bonnet, R., Swingedouw, D., Gastineau, G., Boucher, O., Deshayes, J., Hourdin, F., et al. (2021). Increased risk of near term global warming due to a recent AMOC weakening. *Nature Communications*, *12*(1), 6108. https://doi.org/10.1038/s41467-021-26370-0

Brönnimann, S., Kennedy, J., Rayner, N. A., Samakinwa, E., Valler, V., Hand, R., et al. (2021). An ensemble reconstruction of global monthly sea surface temperature and sea ice concentration 1000–1849 [Dataset]. *Figshare*. https://doi.org/10.6084/m9.figshare.c.5369309.v1

Buckley, M. W., & Marshall, J. (2016). Observations, inferences, and mechanisms of the Atlantic meridional overturning circulation: A review. *Reviews of Geophysics*, *54*(1), 5–63. https://doi.org/10.1002/2015RG000493

Cleveland Stout, R., Proistosescu, C., & Roe, G. (2023). Fingerprinting low-frequency last millennium temperature variability in forced and unforced climate models. *Journal of Climate*, *36*(20), 7005–7023. https://doi.org/10.1175/JCLI-D-22-0810.1

Cornish, S. B., Kostov, Y., Johnson, H. L., & Lique, C. (2020). Response of Arctic freshwater to the Arctic oscillation in coupled climate models. *Journal of Climate*, *33*(7), 2533–2555. https://doi.org/10.1175/JCLI-D-19-0685.1

Delworth, T. L., & Zeng, F. (2012). Multicentennial variability of the Atlantic meridional overturning circulation and its climatic influence in a 4000 year simulation of the GFDL CM2.1 climate model. *Geophysical Research Letters*, *39*(13), L13702. https://doi.org/10.1029/2012GL052107

de Vries, P., & Weber, S. L. (2005). The Atlantic freshwater budget as a diagnostic for the existence of a stable shut down of the meridional overturning circulation. *Geophysical Research Letters*, *32*(9). https://doi.org/10.1029/2004GL021450

Dodd, P. A., Heywood, K. J., Meredith, M. P., Naveira-Garabato, A. C., Marca, A. D., & Falkner, K. K. (2009). Sources and fate of freshwater exported in the East Greenland Current. *Geophysical Research Letters*, *36*(19). https://doi.org/10.1029/2009GL039663

Döscher, R., Acosta, M., Alessandri, A., Anthoni, P., Arsouze, T., Bergman, T., et al. (2022). The EC-Earth3 Earth system model for the coupled model intercomparison Project 6. *Geoscientific Model Development*, *15*(7), 2973–3020. https://doi.org/10.5194/gmd-15-2973-2022

Drijfhout, S. S., Weber, S. L., & van der Swaluw, E. (2011). The stability of the MOC as diagnosed from model projections for pre-industrial, present and future climates. *Climate Dynamics*, *37*(7–8), 1575–1586. https://doi.org/10.1007/s00382-010-0930-z

Ebisuzaki, W. (1997). A method to estimate the statistical significance of a correlation when the data are serially correlated. *Journal of Climate*, *10*(9), 2147–2153. https://doi.org/10.1175/1520-0442(1997)010⟨2147:AMTETS⟩2.0.CO;2

Ellerhoff, B., Kirschner, M. J., Ziegler, E., Holloway, M. D., Sime, L., & Rehfeld, K. (2022). Contrasting state-dependent effects of natural forcing on global and local climate variability. *Geophysical Research Letters*, *49*(10). https://doi.org/10.1029/2022GL098335

Eyring, V., Bony, S., Meehl, G. A., Senior, C. A., Stevens, B., Stouffer, R. J., & Taylor, K. E. (2016). Overview of the Coupled Model Intercomparison Project Phase 6 (CMIP6) experimental design and organization. *Geoscientific Model Development*, *9*(5), 1937–1958. https://doi.org/10.5194/gmd-9-1937-2016

Eyring, V., Gillett, N., Achuta Rao, K., Barimalala, R., Barreiro Parrillo, M., Bellouin, N., et al. (2021). Human influence on the climate system. In V. Masson-Delmotte, et al. (Ed.), *Climate change 2021: The physical science basis. Contribution of working group I to the sixth assessment report of the intergovernmental panel on climate change* (pp. 423–552). Cambridge University Press. https://doi.org/10.1017/9781009157896.005

Fabiano, F., Davini, P., Meccia, V. L., Zappa, G., Bellucci, A., Lembo, V., et al. (2024). Multi-centennial evolution of the climate response and deep-ocean heat uptake in a set of abrupt stabilization scenarios with EC-Earth3. *Earth System Dynamics*, *15*(2), 527–546. https://doi.org/10.5194/esd-15-527-2024

GEBCO Bathymetric Compilation Group. (2023). The GEBCO_2023 grid—A continuous terrain model of the global oceans and land [Dataset]. *NERC EDS British Oceanographic Data Centre NOC*. https://doi.org/10.5285/F98B053B-0CBC-6C23-E053-6C86ABC0AF7B

Haine, T. W. N., Curry, B., Gerdes, R., Hansen, E., Karcher, M., Lee, C., et al. (2015). Arctic freshwater export: Status, mechanisms, and prospects. *Global and Planetary Change*, *125*, 13–35. https://doi.org/10.1016/j.gloplacha.2014.11.013

Heuzé, C. (2021). Antarctic bottom water and North Atlantic deep water in CMIP6 models. *Ocean Science*, *17*(1), 59–90. https://doi.org/10.5194/os-17-59-2021

Jiang, W., Gastineau, G., & Codron, F. (2021). Multicentennial variability driven by salinity exchanges between the Atlantic and the Arctic Ocean in a coupled climate model. *Journal of Advances in Modeling Earth Systems*, *13*(3), e2020MS002366. https://doi.org/10.1029/2020MS002366

Jungclaus, J. H., Bard, E., Baroni, M., Braconnot, P., Cao, J., Chini, L. P., et al. (2017). The PMIP4 contribution to CMIP6 – Part 3: The last millennium, scientific objective, and experimental design for the PMIP4 Past1000 simulations. *Geoscientific Model Development*, *10*(11), 4005–4033. https://doi.org/10.5194/gmd-10-4005-2017

Jungclaus, J. H., Haak, H., Latif, M., & Mikolajewicz, U. (2005). Arctic–North Atlantic interactions and multidecadal variability of the meridional overturning circulation. *Journal of Climate*, *18*(19), 4013–4031. https://doi.org/10.1175/JCLI3462.1

Kelson, R. L., Straub, D. N., & Dufour, C. O. (2022). Using CMIP6 models to assess the significance of the observed trend in the Atlantic meridional overturning circulation. *Geophysical Research Letters*, *49*(20), e2022GL100202. https://doi.org/10.1029/2022GL100202

Kim, H.-J., An, S.-I., Park, J.-H., Sung, M.-K., Kim, D., Choi, Y., & Kim, J.-S. (2023). North Atlantic oscillation impact on the Atlantic meridional overturning circulation shaped by the mean state. *npj Climate and Atmospheric Science*, *6*, 25. https://doi.org/10.1038/s41612-023-00354-x

Klockmann, M., Mikolajewicz, U., & Marotzke, J. (2018). Two AMOC states in response to decreasing greenhouse gas concentrations in the coupled climate model MPI-ESM. *Journal of Climate*, *31*(19), 7969–7984. https://doi.org/10.1175/JCLI-D-17-0859.1

Knight, J. R., Allan, R. J., Folland, C. K., Vellinga, M., & Mann, M. E. (2005). A signature of persistent natural thermohaline circulation cycles in observed climate. *Geophysical Research Letters*, *32*(20). https://doi.org/10.1029/2005GL024233

Laepple, T., Ziegler, E., Weitzel, N., Hébert, R., Ellerhoff, B., Schoch, P., et al. (2023). Regional but not global temperature variability underestimated by climate models at supradecadal timescales. *Nature Geoscience*, *16*(11), 1–9. https://doi.org/10.1038/s41561-023-01299-9

Lehner, F., Deser, C., Maher, N., Marotzke, J., Fischer, E. M., Brunner, L., et al. (2020). Partitioning climate projection uncertainty with multiple large ensembles and CMIP5/6. *Earth System Dynamics*, *11*(2), 491–508. https://doi.org/10.5194/esd-11-491-2020

Li, Y., & Yang, H. (2022). A theory for self-sustained multicentennial oscillation of the Atlantic meridional overturning circulation. *Journal of Climate*, *35*(18), 5883–5896. https://doi.org/10.1175/JCLI-D-21-0685.1

Lippold, J., Pöppelmeier, F., Süfke, F., Gutjahr, M., Goepfert, T. J., Blaser, P., et al. (2019). Constraining the variability of the Atlantic meridional overturning circulation during the Holocene. *Geophysical Research Letters*, *46*(20), 11338–11346. https://doi.org/10.1029/2019GL084988

Little, C. M., Zhao, M., & Buckley, M. W. (2020). Do surface temperature indices reflect centennial-timescale trends in Atlantic meridional overturning circulation strength? *Geophysical Research Letters*, *47*(22), e2020GL090888. https://doi.org/10.1029/2020GL090888

MacMartin, D. G., Zanna, L., & Tziperman, E. (2016). Suppression of Atlantic meridional overturning circulation variability at increased CO_2. *Journal of Climate*, *29*(11), 4155–4164. https://doi.org/10.1175/JCLI-D-15-0533.1

Malmierca-Vallet, I., Sime, L. C., Valdes, P. J., Klockmann, M., Vettoretti, G., & Slattery, J. (2024). The impact of CO_2 and climate state on whether Dansgaard–Oeschger type oscillations occur in climate models. *Geophysical Research Letters*, *51*(13), e2024GL110068. https://doi.org/10.1029/2024GL110068

Mann, M. E., & Lees, J. M. (1996). Robust estimation of background noise and signal detection in climatic time series. *Climatic Change*, *33*(3), 409–445. https://doi.org/10.1007/BF00142586

Martin, T., Park, W., & Latif, M. (2015). Southern Ocean forcing of the North Atlantic at multi-centennial time scales in the Kiel climate model. *Deep Sea Research. II*, *114*, 39–48. https://doi.org/10.1016/j.dsr2.2014.01.018

Meccia, V. L., Fuentes-Franco, R., Davini, P., Bellomo, K., Fabiano, F., Yang, S., & von Hardenberg, J. (2023). Internal multi-centennial variability of the Atlantic meridional overturning circulation simulated by EC-Earth3. *Climate Dynamics*, *60*(11–12), 3695–3712. https://doi.org/10.1007/s00382-022-06534-4

Mehling, O. (2024). Analysis code for "Centennial-scale variability of the Atlantic Meridional Overturning Circulation in CMIP6 models shaped by Arctic–North Atlantic interactions and sea ice biases" [Software]. *Zenodo*. https://doi.org/10.5281/zenodo.11640570

Mehling, O., Bellomo, K., Angeloni, M., Pasquero, C., & von Hardenberg, J. (2023). High-latitude precipitation as a driver of multicentennial variability of the AMOC in a climate model of intermediate complexity. *Climate Dynamics*, *61*(3–4), 1519–1534. https://doi.org/10.1007/s00382-022-06640-3

Menary, M. B., Hodson, D. L. R., Robson, J. I., Sutton, R. T., Wood, R. A., & Hunt, J. A. (2015). Exploring the impact of CMIP5 model biases on the simulation of North Atlantic decadal variability. *Geophysical Research Letters*, *42*(14), 5926–5934. https://doi.org/10.1002/2015GL064360

Menary, M. B., Park, W., Lohmann, K., Vellinga, M., Palmer, M. D., Latif, M., & Jungclaus, J. H. (2012). A multimodel comparison of centennial Atlantic meridional overturning circulation variability. *Climate Dynamics*, *38*(11–12), 2377–2388. https://doi.org/10.1007/s00382-011-1172-4

Mignot, J., Hourdin, F., Deshayes, J., Boucher, O., Gastineau, G., Musat, I., et al. (2021). The tuning strategy of IPSL-CM6A-LR. *Journal of Advances in Modeling Earth Systems*, *13*(5), e2020MS002340. https://doi.org/10.1029/2020MS002340

Moffa-Sánchez, P., Moreno-Chamarro, E., Reynolds, D. J., Ortega, P., Cunningham, L., Swingedouw, D., et al. (2019). Variability in the northern North Atlantic and Arctic oceans across the last two Millennia: A review. *Paleoceanography and Paleoclimatology*, *34*(8), 1399–1436. https://doi.org/10.1029/2018PA003508

Mudelsee, M. (2014). *Climate time series analysis* (2nd ed.), Springer.

Muir, L. C., & Fedorov, A. V. (2015). How the AMOC affects ocean temperatures on decadal to centennial timescales: The North Atlantic versus an interhemispheric seesaw. *Climate Dynamics*, *45*(1–2), 151–160. https://doi.org/10.1007/s00382-014-2443-7

Pan, R., Shu, Q., Wang, Q., Wang, S., Song, Z., He, Y., & Qiao, F. (2023). Future Arctic climate change in CMIP6 strikingly intensified by NEMO-family climate models. *Geophysical Research Letters*, *50*(4), e2022GL102077. https://doi.org/10.1029/2022GL102077

Parsons, L. A., Brennan, M. K., Wills, R. C., & Proistosescu, C. (2020). Magnitudes and spatial patterns of interdecadal temperature variability in CMIP6. *Geophysical Research Letters*, *47*(7), e2019GL086588. https://doi.org/10.1029/2019GL086588

Patrizio, C. R., Athanasiadis, P. J., Frankignoul, C., Iovino, D., Masina, S., Paolini, L. F., & Gualdi, S. (2023). Improved extratropical North Atlantic atmosphere–ocean variability with increasing ocean model resolution. *Journal of Climate*, *36*(24), 8403–8424. https://doi.org/10.1175/JCLI-D-23-0230.1

Percival, D. B., & Walden, A. T. (2020). *Spectral analysis for univariate time series*. Cambridge University Press.

Prange, M., Jonkers, L., Merkel, U., Schulz, M., & Bakker, P. (2023). A multicentennial mode of North Atlantic climate variability throughout the last Glacial maximum. *Science Advances*, *9*(44), eadh1106. https://doi.org/10.1126/sciadv.adh1106

Reintges, A., Robson, J. I., Sutton, R., & Yeager, S. G. (2024). Subpolar North Atlantic mean state affects the response of the Atlantic meridional overturning circulation to the North Atlantic oscillation in CMIP6 models. *Journal of Climate*, *37*(21), 5543–5559. https://doi.org/10.1175/JCLI-D-23-0470.1

Rugenstein, M., Bloch-Johnson, J., Abe-Ouchi, A., Andrews, T., Beyerle, U., Cao, L., et al. (2019). LongRunMIP: Motivation and design for a large collection of millennial-length AOGCM simulations. *Bulletin of the American Meteorological Society*, *100*(12), 2551–2570. https://doi.org/10.1175/BAMS-D-19-0068.1

Samakinwa, E., Valler, V., Hand, R., Neukom, R., Gómez-Navarro, J. J., Kennedy, J., et al. (2021). An ensemble reconstruction of global monthly sea surface temperature and sea ice concentration 1000–1849. *Scientific Data*, *8*(1), 261. https://doi.org/10.1038/s41597-021-01043-1

Shu, Q., Wang, Q., Guo, C., Song, Z., Wang, S., He, Y., & Qiao, F. (2023). Arctic Ocean simulations in the CMIP6 Ocean Model Intercomparison Project (OMIP). *Geoscientific Model Development*, *16*(9), 2539–2563. https://doi.org/10.5194/gmd-16-2539-2023

Thomson, D. (1982). Spectrum estimation and harmonic analysis. *Proceedings of the IEEE*, *70*(9), 1055–1096. https://doi.org/10.1109/PROC.1982.12433

van Westen, R. M., & Dijkstra, H. A. (2023). Asymmetry of AMOC hysteresis in a state-of-the-art global climate model. *Geophysical Research Letters*, *50*(22), e2023GL106088. https://doi.org/10.1029/2023GL106088

van Westen, R. M., & Dijkstra, H. A. (2024). Persistent climate model biases in the Atlantic Ocean's freshwater transport. *Ocean Science*, *20*(2), 549–567. https://doi.org/10.5194/os-20-549-2024

Vellinga, M., & Wu, P. (2004). Low-latitude freshwater influence on centennial variability of the Atlantic thermohaline circulation. *Journal of Climate*, *17*(23), 4498–4511. https://doi.org/10.1175/3219.1

von der Heydt, A. S., Ashwin, P., Camp, C. D., Crucifix, M., Dijkstra, H. A., Ditlevsen, P., & Lenton, T. M. (2021). Quantification and interpretation of the climate variability record. *Global and Planetary Change*, *197*, 103399. https://doi.org/10.1016/j.gloplacha.2020.103399

Waldman, R., Hirschi, J., Voldoire, A., Cassou, C., & Msadek, R. (2021). Clarifying the relation between AMOC and thermal Wind: Application to the centennial variability in a coupled climate model. *Journal of Physical Oceanography*, *51*(2), 343–364. https://doi.org/10.1175/JPO-D-19-0284.1

Wei, X., & Zhang, R. (2022). A simple conceptual model for the self-sustained Multidecadal AMOC variability. *Geophysical Research Letters*, *49*(14), e2022GL099800. https://doi.org/10.1029/2022GL099800

Weijer, W., Cheng, W., Drijfhout, S. S., Fedorov, A. V., Hu, A., Jackson, L. C., et al. (2019). Stability of the Atlantic meridional overturning circulation: A review and synthesis. *Journal of Geophysical Research: Oceans*, *124*(8), 5336–5375. https://doi.org/10.1029/2019JC015083

Yang, K., Yang, H., Li, Y., & Zhang, Q. (2024). North Atlantic ocean-originated multicentennial oscillation of the AMOC: A coupled model study. *Journal of Climate*, *37*(9), 2789–2807. https://doi.org/10.1175/JCLI-D-23-0422.1

Zanowski, H., Jahn, A., & Holland, M. M. (2021). Arctic Ocean freshwater in CMIP6 ensembles: Declining Sea Ice, increasing ocean storage and export. *Journal of Geophysical Research: Oceans*, *126*(4), e2020JC016930. https://doi.org/10.1029/2020JC016930

Zhang, R., & Thomas, M. (2021). Horizontal circulation across density surfaces contributes substantially to the long-term mean Northern Atlantic Meridional Overturning Circulation. *Communications Earth & Environment*, *2*, 112. https://doi.org/10.1038/s43247-021-00182-y

Zhao, A., Robson, J., Sutton, R., Lai, M. W., Mecking, J. V., Yeager, S., & Petit, T. (2024). Large diversity in AMOC internal variability across NEMO-based climate models. *Climate Dynamics*, *62*(5), 3355–3374. https://doi.org/10.1007/s00382-023-07069-y

References From the Supporting Information

Boucher, O., Denvil, S., Levavasseur, G., Cozic, A., Caubel, A., Foujols, M.-A., et al. (2018). IPSL IPSL-CM6A-LR model output prepared for CMIP6 CMIP piControl [Dataset]. *Earth System Grid Federation*. https://doi.org/10.22033/ESGF/CMIP6.5251

Boucher, O., Servonnat, J., Albright, A. L., Aumont, O., Balkanski, Y., Bastrikov, V., et al. (2020). Presentation and evaluation of the IPSL-cm6a-LR climate model. *Journal of Advances in Modeling Earth Systems*, *12*(7), e2019MS002010. https://doi.org/10.1029/2019MS002010

Danabasoglu, G., Lamarque, J.-F., Bacmeister, J., Bailey, D. A., DuVivier, A. K., Edwards, J., et al. (2020). The Community Earth System Model Version 2 (CESM2). *Journal of Advances in Modeling Earth Systems*, *12*, e2019MS001916. https://doi.org/10.1029/2019MS001916

Danabasoglu, G., Lawrence, D., Lindsay, K., Lipscomb, W., & Strand, G. (2019). NCAR CESM2 model output prepared for CMIP6 CMIP piControl [Dataset]. *Earth System Grid Federation*. https://doi.org/10.22033/ESGF/CMIP6.7733

EC-Earth Consortium. (2019). EC-Earth-Consortium EC-Earth3 model output prepared for CMIP6 CMIP piControl [Dataset]. *Earth System Grid Federation*. https://doi.org/10.22033/ESGF/CMIP6.4842

Kuhlbrodt, T., Jones, C. G., Sellar, A., Storkey, D., Blockley, E., Stringer, M., et al. (2018). The low-resolution version of HadGEM3 GC3.1: Development and evaluation for global climate. *Journal of Advances in Modeling Earth Systems*, *10*(11), 2865–2888. https://doi.org/10.1029/2018MS001370

Mauritsen, T., Bader, J., Becker, T., Behrens, J., Bittner, M., Brokopf, R., et al. (2019). Developments in the MPI-M Earth System Model Version 1.2 (MPI-ESM1.2) and its response to increasing CO_2. *Journal of Advances in Modeling Earth Systems*, *11*(4), 998–1038. https://doi.org/10.1029/2018MS001400

Neubauer, D., Ferrachat, S., Siegenthaler-Le Drian, C., Stoll, J., Folini, D. S., Tegen, I., et al. (2019). HAMMOZ-Consortium MPI-ESM1.2-HAM model output prepared for CMIP6 CMIP piControl [Dataset]. *Earth System Grid Federation*. https://doi.org/10.22033/ESGF/CMIP6.5037

Ridley, J., Menary, M., Kuhlbrodt, T., Andrews, M., & Andrews, T. (2018). MOHC HadGEM3-GC31-LL model output prepared for CMIP6 CMIP piControl [Dataset]. *Earth System Grid Federation*. https://doi.org/10.22033/ESGF/CMIP6.6294

Sellar, A. A., Jones, C. G., Mulcahy, J. P., Tang, Y., Yool, A., Wiltshire, A., et al. (2019). UKESM1: Description and evaluation of the U.K. Earth system model. *Journal of Advances in Modeling Earth Systems*, *11*(12), 4513–4558. https://doi.org/10.1029/2019MS001739

Swart, N. C., Cole, J. N., Kharin, V. V., Lazare, M., Scinocca, J. F., Gillett, N. P., et al. (2019b). CCCma CanESM5 model output prepared for CMIP6 CMIP piControl [Dataset]. *Earth System Grid Federation*. https://doi.org/10.22033/ESGF/CMIP6.3673

Swart, N. C., Cole, J. N. S., Kharin, V. V., Lazare, M., Scinocca, J. F., Gillett, N. P., et al. (2019a). The Canadian Earth System Model Version 5 (CanESM5.0.3). *Geoscientific Model Development*, *12*(11), 4823–4873. https://doi.org/10.5194/gmd-12-4823-2019

Tang, Y., Rumbold, S., Ellis, R., Kelley, D., Mulcahy, J., Sellar, A., et al. (2019). MOHC UKESM1.0-LL model output prepared for CMIP6 CMIP piControl [Dataset]. *Earth System Grid Federation*. https://doi.org/10.22033/ESGF/CMIP6.6298

Tegen, I., Neubauer, D., Ferrachat, S., Siegenthaler-Le Drian, C., Bey, I., Schutgens, N., et al. (2019). The global aerosol–climate model ECHAM6.3–HAM2.3 – Part 1: Aerosol evaluation. *Geoscientific Model Development*, *12*(4), 1643–1677. https://doi.org/10.5194/gmd-12-1643-2019

Walsh, J. E., Chapman, W. L., Fetterer, F., & Stewart, J. S. (2019). Gridded monthly Sea Ice extent and concentration, 1850 Onward, version 2 [Dataset]. *NSIDC: National Snow and Ice Data Center*. https://doi.org/10.7265/jj4s-tq79

Walsh, J. E., Fetterer, F., Stewart, J. S., & Chapman, W. L. (2017). A database for depicting Arctic sea ice variations back to 1850. *Geography Review*, *107*, 89–107. https://doi.org/10.1111/j.1931-0846.2016.12195.x

Wieners, K.-H., Giorgetta, M., Jungclaus, J., Reick, C., Esch, M., Bittner, M., et al. (2019). MPI-M MPI-ESM1.2-LR model output prepared for CMIP6 CMIP piControl [Dataset]. *Earth System Grid Federation*. https://doi.org/10.22033/ESGF/CMIP6.6675

Ziehn, T., Chamberlain, M., Lenton, A., Law, R., Bodman, R., Dix, M., et al. (2019). CSIRO ACCESS-ESM1.5 model output prepared for CMIP6 CMIP piControl [Dataset]. *Earth System Grid Federation*. https://doi.org/10.22033/ESGF/CMIP6.4312

Ziehn, T., Chamberlain, M. A., Law, R. M., Lenton, A., Bodman, R. W., Dix, M., et al. (2020). The Australian Earth system model: ACCESS-ESM1.5. *Journal of Southern Hemisphere Earth Systems Science*, *70*(1), 193–214. https://doi.org/10.1071/ES19035